The Astronomical Journal, 134:1923–1933, 2007 November

A STATISTICAL STUDY OF ACCRETION DISK MODEL SPECTRA FOR CATACLYSMIC VARIABLES

Raúl E. Puebla and Marcos P. Diaz
Instituto de Astronomia, Geofísica, e Ciências Atmosféricas, Universidade de São Paulo, Rua de Matão 1226,
Cidade Universitária, 05508-900 São Paulo, SP, Brazil; raul@astro.iag.usp.br, marcos@astro.iag.usp.br

and

Ivan Hubeny
Department of Astronomy, Steward Observatory, The University of Arizona, 933 North Cherry Avenue,
Tucson, AZ 85721-0065, USA; hubeny@as.arizona.edu
Received 2007 April 4; accepted 2007 August 3

ABSTRACT

We have performed a statistical test of the currently used accretion disk models for cataclysmic variables (CVs) using a set of 33 CVs with steady disks (10 old novae and 23 nova-like systems). The mass transfer rate ($\dot{M}$) for each system was also calculated. Ultraviolet (UV) data were fitted by model spectra using a multiparametric optimization method, aiming to constrain the $\dot{M}$ values. It was verified that these accretion disk models fail to fit both color and flux simultaneously, as previously noted when composite stellar atmosphere models were fitted to the UV spectra of CVs by Wade. By applying such models to a sample of novae and nova-like CVs, we confirm that the limb-darkening effect must be taken into account when estimating mass transfer rates, especially for high-inclination systems. Important fitting degeneracies of the basic disk parameters are analyzed. Our simulations suggest that to reproduce the observations a revision of the temperature profile, at least in the innermost parts of the disk, seems to be required, and possibly the vertical distribution of the viscosity should be revised. In addition, an optically thin layer or an extended disk component should be considered. This component may be physically represented by a disk wind and/or a chromosphere. A physical description of the emission-line profiles may help to break the degeneracies that appear when only the continuum is analyzed. The average value of $\dot{M}$ found for nova-like systems is $\sim 9.3 \times 10^{-9}\ M_{\odot}\ \mathrm{yr}^{-1}$, while $\sim 1.3 \times 10^{-8}\ M_{\odot}\ \mathrm{yr}^{-1}$ is found for old classical novae. No clear evidence is found for either the presence or absence of a correlation between $\dot{M}$ and the orbital period. Such correlation analysis was performed for high accretion rate systems (15 nova-like systems and 10 old novae), but we were not able to find a well-defined correlation as found by Patterson. By measuring the equivalent width of the emission lines (C IV λ1550 and He II λ1640) we found a lack of systems with low $\dot{M}$ and strong UV emission lines. A correlation between the equivalent width of such lines and the orbital inclination (i) was also confirmed.

Key words: accretion, accretion disks — novae, cataclysmic variables — ultraviolet: general

1. INTRODUCTION

Nonmagnetic cataclysmic variables (CVs) are semidetached binary systems in which a Roche lobe–filling star transfers mass onto a white dwarf (WD), or primary, through an accretion disk. The secondary star is close to the main sequence for most CVs. Commonly, the disk is the most luminous element in the system, especially for nova-like systems and old classical novae. These CV types show a steady continuum radiation that comes from the disk's surface, which dominates the ultraviolet and visible spectra. They are the brightest type of CVs and have been widely used to study the properties of accretion disks in binary systems. For decades several disk models and methods of spectral synthesis have been developed trying to fit the observed spectra. In the first attempts the disk was approximated by a superposition of blackbody radiating rings that obeyed the standard temperature radial distribution (eq. [1]) (Lynden-Bell 1969; Lynden-Bell & Pringle 1974; Tylenda 1977; Pringle 1981; La Dous 1989). In the case of an infinite disk the spectral energy distribution takes the well-known form $f_{\lambda} \propto \lambda^{-2.33}$ (Lynden-Bell 1969). Subsequently, in order to reproduce the emission lines observed in the optical and UV spectra, the disk was assumed to be optically thin in the vertical direction, or an optically thin layer was added, keeping a homogeneous vertical structure (Tylenda 1981; Williams 1980; Williams & Ferguson 1982; Williams & Shipman 1988). The observed resonance lines in the UV may correspond to high-ionization states that are Doppler-widened. A P Cygni profile with a wide and deep absorption component is often present in systems with low orbital inclination, which would be evidence of the presence of a wind arising from the disk. The disk regions capable of driving a wind with the observed velocities ($\sim$3000–5000 km s^{-1}) would be the inner disk and/or the boundary layer (BL). Patterson & Raymond (1985) found a correlation between the He II (λ4686) emission-line intensity and the X-ray flux, but they did not find the same correlation for He II (λ1640). The hybrid disk/chromosphere models by Ko et al. (1996) suggest that in order to explain the intensity of the emission lines, significant disk irradiation by the BL is necessary.

Other kinds of models have been developed in order to reproduce the shape of the continuum and absorption lines using the approximation of an optically thick disk. The first models of this type made use of Kurucz (1979) atmospheres. Although these models describe a few spectral details, they present problems when the observed data are fitted over a broad wavelength range (Wade 1984, 1988; Verbunt 1997). The latest generation of models are solved for the whole vertical structure of the disk, assuming that the disk properties vary much faster in the vertical than in the radial direction. Computing the model vertical structure for a given radial distance resembles computing a model stellar atmosphere; the approach thus gained the name "disk atmospheres." However,

although this term is widely used, it is quite misleading, because it suggests that one considers only the outer layer (atmosphere) of a disk, while in fact the whole disk is being treated. Unlike the standard atmosphere models, these atmospheres take into account the dependence of gravity on depth and the internal generation of energy by viscous processes. Limb darkening is also taken into account (Kriz & Hubeny 1986; Shaviv & Wehrse 1986; Hubeny 1989, 1990a; Diaz et al. 1996; Wade & Hubeny 1998). From the spectral synthesis of such disk atmosphere models, one may extract a few relations between the spectral features and the physical properties of the disk. These models follow the standard disk temperature profile, and therefore, the flux level and continuum shape are strongly coupled to the mass of the white dwarf, the mass accretion rate, and the orbital inclination. The absorption-line intensities and Balmer discontinuity are also affected (La Dous 1989). Due to these dependencies the continuum is widely used to estimate the mass transfer rate, although this estimate requires a measurement of the primary mass by independent methods. The orbital inclination also impacts the flux level and the slope (color) of the continuum emission. In particular, systems with high orbital inclination are strongly affected by limb darkening, as described by Diaz et al. (1996). Although the atmosphere disk models may be better able to describe the disk spectrum features, problems already found using classical atmosphere models (Wade 1988) do persist in the current disk atmosphere models (Diaz & Hubeny 1999). However, these models have been effectively used to study disk properties and to estimate the basic parameters of CVs (e.g., Long et al. 1994; Diaz & Hubeny 1999; Nadalin & Sion 2001; Moyer et al. 2003; Hamilton & Sion 2004; Engle & Sion 2005; Godon et al. 2006). It is worth evaluating to which degree the estimates based on such models are accurate and reliable

In this work we have tested disk atmosphere models using a sample of 33 CVs, by modeling their UV spectra as observed by *IUE* and the *Hubble Space Telescope* (*HST*). We have used a controlled sample of CVs, with the aim of identifying future improvements to the current generation of models. This kind of analysis led us to investigate systematic trends of the model and to discover its weaknesses. We have also calculated $\dot{M}$ using a homogeneous method, trying to reproduce Patterson's (1984) relation between the accretion rate and orbital period using these revised $\dot{M}$ values. This relation is predicted by the most accepted CV evolution theories (e.g., Rappaport et al. 1983; Howell et al. 2001). Nevertheless, it has been tested and criticized as new $\dot{M}$ values have been calculated using different methods (e.g., Verbunt & Wade 1984; King 1996). Warner (1987) suggested that this correlation would actually be the product of a selection effect caused by the strong dependence of the secondary star absolute magnitude M_V on the orbital period (Patterson 1984). More recently, Rutten et al. (1992) calculated $\dot{M}$ for a set of six cataclysmic stars. They did not find such a correlation. However, it is difficult to derive statistically reliable conclusions from the small sample employed in that study. It is also relevant to analyze the stability of the disks in our sample, since there exists, according to the disk instability model (DIM; see Lasota 2001 for a review), conditions that limit the $\dot{M}$ values in order to avoid dwarf nova outbursts, and our disks should fulfill those conditions. We have made an instability analysis of our sample, and the results are shown in § 4.2.1.

In order to reach the goal of constraining $\dot{M}$, one needs to know, among other parameters, the value of M_1, i, and the distance d for each system with reasonable accuracy. The UV spectra were collected from the *IUE* data archive and from STIS and GHRS spectrograph data in the *HST* database. The details of each parameter, their uncertainties, and the UV spectra used in this work are presented in the next section. The disk model and spectral synthesis details, as well as the multiparametric optimization method employed, are described in § 3. The results of the disk model test, including its reach and limitations, as well as the new $\dot{M}$ estimates, are presented in § 4. A brief summary and perspectives are given in § 5.

2. THE DATA

2.1. *Spectral Data*

Only UV spectra were used in the presented simulations. We have compiled a sample of steady CVs with known orbital periods as large as possible that fulfill certain conditions. Systems with steady behavior such as nova-like systems and old classical novae were selected. Additional criteria were $m_V < 17$ in order to have a reasonable signal-to-noise ratio with *HST* and *IUE*, and orbital inclination $i < 80^\circ$ in order to avoid partial viewing of the inner disk. At least 10 years after the last eruption were required for selection of old novae. Some VY Scl–type nova-like systems in a high state were included in the sample. This search produces a set of 47 CVs. Table 1 shows a list of the systems with their observation dates and data sources.

The main source of UV spectra for this work was the *IUE* satellite database. The selected *IUE* spectra were observed with the SWP and LWP (or LWR) cameras on the same date, or on very close dates. We basically tried to fit the continuum shape. Therefore, a low dispersion and large aperture were chosen in order to obtain the widest spectral coverage, the best flux calibration, and the highest possible signal-to-noise ratio. In this operation mode, the *IUE* spectrograph had a resolution of $\sim$6 Å ($R = 270$ at 1500 Å). The spectral coverage using this instrument is 1150–3350 Å.

Spectra from the *HST* STIS were used for BK Lyn and V794 Aql. The data collected were observed with the grid G140L at first order and the FUV-MAMA detector. Those have a spectral resolution of $\sim$1 Å and coverage from 1150 to 1700 Å.

2.2. *The System Parameters*

In order to generate a meaningful grid of models for each system, it is necessary to know with certain accuracy a few basic system parameters. These parameters were obtained from an extensive search in the published literature (Table 1). The parameters taken from previous studies are the primary mass M_1, the orbital inclination i, the distance d, and the orbital period $P_{\rm orb}$. Furthermore, the spectra need to be corrected for interstellar extinction, since it strongly affects the UV band. The color excess $E(B-V)$ or the interstellar extinction coefficient A_V was used, as well as the standard extinction law of Cardelli et al. (1989). The values found in that search through the literature are shown in Table 1, including an error estimate for each parameter if available. Those parameter values and their errors helped us to constrain the parameter space for which the grid of models for each system was generated. Knowledge of the parameter errors is essential in order to evaluate the errors in the $\dot{M}$ values. In that sense it is important to note that the uncertainty in the primary mass depends strongly on the orbital inclination, being lower for high-inclination and eclipsing systems. In the case of the distance, a multiplicity of methods are employed, but most of them have poor accuracy. For example, completely different distance values were found in the cases of HR Del and RR Pic. This fact points toward a strong dependency of the method on premises that were weak or not verified. As already mentioned, interstellar extinction strongly affects the UV spectra. For instance, the determination of $E(B-V)$ with an error between $\sim$0.02 and 0.05 would produce an error in $\dot{M}$ between $\sim$30% and 50%.

TABLE 1

System Parameters Taken from the Literature for the Selected CVs

Object	P (days)	m_V	Type[a]	i (deg)	M_1 ($M_\odot$)	M_2 ($M_\odot$)	d (pc)	$E(B-V)$	Date Obs.	Ref.
HV And	0.05	15.2	NL						2002 Nov 26	1
CP Pup	0.06	15	CN (1942)	25–35	0.12–0.86		700	0.21	1986 Feb 27	1, 3, 26, 39
V348 Pup	0.1	15.5	NL	81.1 ± 1	0.65	0.2	429–500	0.18–0.40	1991 Apr 15	1, 35
BK Lyn	0.07	14.1	NL	32 ± 12	$0.3^{+0.5}_{-0.12}$	0.2	114–185	0	2003 Apr 13	7, 26
LQ Peg	0.12	13	NL						1982 Jul 6	1
V592 Cas	0.12	12.6	NL	18–39	>0.8	0.3	330	0.25	1981 Dec 5	1, 3, 15, 35
V442 Oph	0.12	14	NL (VY)	67 ± 27	0.34 ± 0.1	0.31 ± 0.02	80–130	0.22	1981 Oct 12	1, 3, 12
DN Gem	0.13	15.8	CN (1912)	<50	1?	0.34	1600 ± 600	0.8–0.13	1990 Feb 19	1, 3, 14
SW Sex	0.13	14.8	NL	>75	0.5	<3	450 ± 10	0	1983 Nov 13	1, 3, 28
HL Aqr	0.14	13.5	NL					0.05	1984 Jun 24	1, 4
DW UMa	0.14	14.9	NL	82 ± 4	0.77 ± 0.07	0.3 ± 0.1	930 ± 160	0	1987 Feb 12	1, 3, 15
LN UMa	0.14	14.6	NL (VY)						1991 Feb 28	1
V603 Aql	0.14	11.4	CN (1918)	13 ± 2	1.2 ± 0.2	0.29 ± 0.4	110–360	0.08	1996 May 7	1, 2, 18, 19
V1315 Aql	0.14	14.4	NL	82 ± 4	0.73 ± 0.3	0.3 ± 0.01	300	0.1	1985 Nov 12	1, 3, 19
WX Ari	0.14	15.3	NL	72		0.32	198		1983 Jan 19	1, 19, 34
BP Lyn	0.15	14.5	NL	60–70	0.2–0.3	0.4–0.42	150–170		1988 Feb 18	1, 10
RR Pic	0.15	12	CN (1925)	65	0.95	0.4	600/240	0.02	1982 Aug 23	1, 2, 17, 18, 42
PX And	0.15	15	NL	74	0.7?	0.32	>180	0.05	1990 Jul 21	1, 25, 26
V533 Her	0.15	14.3	CN (1963)	62	0.95	0.33	1200	0.03	1992 May 29	1, 3, 19, 36
V794 Aql	0.15	14.2	NL	39 ± 17	0.88 ± 0.39	0.53 ± 0.07	200	0	2003 Aug 28	1, 3, 25
UU Aqr	0.16	13.3	NL	78 ± 2	0.67 ± 0.14	0.2 ± 0.07	200–270		1994 Jun 29	1, 31
BH Lyn	0.16	17.2	NL	79^{+5}_{-3}	$0.73^{+0.7}_{-0.36}$	$0.33^{+0.17}_{-0.11}$			1995 Nov 16	1, 9
LX Ser	0.16	14.5	NL (VY)	75–90	0.41 ± 0.09	0.36 ± 0.02	145–460	0	1985 Feb 26	1, 19, 28
V380 Oph	0.16	15.5	NL	42 ± 13	0.58 ± 0.19	0.36 ± 0.04			2003 Jul 6	1
CM Del	0.16	13.4	NL	73 ± 47	0.48 ± 0.15	0.36 ± 0.03	130–300	0.08	1981 Oct 17	1, 3, 12
V1776 Cyg	0.16	16.7	NL	75	0.6	0.37			1995 Sep 14	1
KR Aur	0.16	11.3	NL (VY)	38 ± 10	0.59 ± 0.17	0.35 ± 0.02	180	0.05	1981 Aug 12	1, 3, 45
LS Peg	0.17	13	NL	30	0.75	0.39		<0.05	1990 Oct 06	1, 23, 24
IX Vel	0.19	9.1	NL	60 ± 5	0.82 ± 0.14	0.53 ± 0.09	95	0.01	1983 Apr 19	1, 3, 17, 21
UX UMa	0.2	12.7	NL	71 ± 0.6	0.47 ± 0.07	0.47 ± 0.1	340	0.02	1982 Feb 16	1, 3, 32
T Aur	0.2	14.9	CN (1891)	57	0.68	0.63	960	0.39	1983 Nov 15	1, 2, 17
HR Del	0.21	11.9	CN (1967)	40 ± 2	0.67 ± 0.08	0.55 ± 0.03	900/285	0.15	1988 Apr 29	1, 2, 22, 42
V825 Her	0.21	14.1	NL						1982 Jul 4	1
V3885 Sgr	0.22	9.6	NL	<50	0.8 ± 0.2	0.7 ± 0.1	110–280	0.02	1984 Apr 10–12	1, 3, 17, 19
V347 Pup	0.23	13.4	NL	80 ± 3	0.63	0.57	510 ± 160	0.05	1991 Apr 15	44
VY Scl	0.23	12.9	NL (VY)	30 ± 10	1.22 ± 0.22	0.43 ± 0.13	530	0.06	1987 Dec 21	1, 3, 19
RW Tri	0.23	12.6	NL	70.5 ± 2.5	0.55 ± 0.15	0.35 ± 0.05	311–379	0.1	1982 Jan 14	1, 3, 16
RW Sex	0.25	10.4	NL	34 ± 6	0.8	0.6	150/400	0.02	1985 Jun 29	1, 3, 27
TW Pic	0.27	14.1	NL (VY)	26–40	<1	0.6	720	0.02	1988 Aug 24	1, 3, 28, 29, 30
AC Cnc	0.3	13.8	NL	72 ± 3	0.76 ± 0.03	0.77 ± 0.05	550 ± 150	0	1982 Dec 5	1, 3, 8
V363 Aur	0.32	14.2	NL	70 ± 2	0.86 ± 0.08	0.77 ± 0.04	600–700 ± 250	0.13	1985 Feb 28	1, 3, 8, 19
BT Mon	0.33	15.4	CN (1939)	82.3 ± 3.2	1.04 ± 0.06	0.87 ± 0.06	1700 ± 300	0.15	1986 Feb 16	1, 6, 11
RZ Gru	0.36	12.3	NL				440 ± 40	0.03	1982 Sep 6–12	1, 3, 20
QU Car	0.45	11.1	NL	<60	~1		610?	0.1	1991 Jun 27	1, 3, 17
DI Lac	0.54	14.3	CN (1910)	<18	0.55–0.8		1320	0.41	1986 Sep 28	1, 2, 13, 42
V841 Oph	0.6	13.5	CN (1848)	8–68	<1.3	<1.3	255	0.3–0.39	1980 Feb 14	1, 2, 19, 37, 38
X Ser	1.48	16.4	CN (1903)					1	1989 May 20	1, 33

Notes.—The columns are object name, orbital period P, apparent magnitude, orbital inclination, primary mass, secondary mass, interstellar extinction $E(B-V)$, and observation date.

[a] (NL) Nova-like system; (CN) classical nova.

References.—(1) Ritter & Kolb 2003; (2) Diaz & Bruch 1997; (3) Bruch & Engel 1994; (4) Hunger et al. 1985; (5) Taylor et al. 1998; (6) Downes & Duerbeck 2000; (7) Dobrzycka & Howell 1992; (8) Thoroughgood et al. 2004; (9) Hoard & Szkody 1997; (10) Hoard & Szkody 1996; (11) Smith et al. 1998; (12) Berriman et al. 1985; (13) Moyer et al. 2003; (14) Retter et al. 1999; (15) Araujo-Betancor et al. 2003; (16) McArthur et al. 1999; (17) Duerbeck 1999; (18) Barret 1996; (19) Meliani et al. 2000; (20) Stickland et al. 1984; (21) Long et al. 1994; (22) Selvelli & Friedjung 2003; (23) Szkody et al. 1997; (24) Taylor et al. 1999; (25) Greiner 1998; (26) Retter & Naylor 2000; (27) Prinja et al. 2003; (28) Rutten et al. 1992; (29) Buckley & Tuohy 1990; (30) Mouchet et al. 1991; (31) Baptista et al. 1996; (32) Patterson 1984; (33) Weight et al. 1994; (34) Rodríguez-Gil et al. 2000; (35) Froming et al. 2003; (36) Rodríguez-Gil & Martinez 2002; (37) Huber et al. 1998; (38) Diaz & Ribeiro 2003; (39) Verbunt et al. 1997; (40) Eracleous et al. 1991; (41) Vande et al. 2003; (42) Warner 1987; (43) Greenstein & Oke 1982; (44) Diaz & Hubeny 1999; (45) Wade 1988.

3. METHODS

3.1. *Disk Model*

The disk model used in this work has been widely described and discussed in the literature (Hubeny 1989, 1990a, 1990b; Diaz et al. 1996; Wade & Hubeny 1998). This model describes a steady, Keplerian-rotating, geometrically thin, optically thick disk, which is divided into a set of concentric rings. Each of these rings radiates like a modified stellar atmosphere, such as mentioned in § 1, and has an effective temperature following the standard disk model temperature law:

$$T(R) = \left(\frac{3GM_1\dot{M}}{8\pi\sigma R_1^3}\right)^{1/4}\left(\frac{R_1}{r}\right)^{3/4}\left[1-\left(\frac{R_1}{r}\right)^{1/2}\right]^{1/4} \quad (1)$$

(see Shakura & Sunyaev 1973; Lynden-Bell & Pringle 1974), where R_1 is the compact star radius, σ is the Stefan-Boltzmann constant, and G is the gravitational constant. The vertical structure of each ring is calculated assuming a plane-parallel atmosphere in hydrostatic equilibrium. The gravity is depth-dependent and arises from the vertical component of the compact star gravitational force. The depth dependence of the internal viscosity dissipation is parameterized through ζ as a power law, given by equations (2) and (3):

$$w(m) = \bar{w}(\zeta+1)\left(\frac{2m}{\Sigma}\right)^{\zeta}, \quad (2)$$

$$\bar{w} = \frac{(GM_1R)^{1/2}}{\mathrm{Re}}, \quad (3)$$

where $\bar{w}$ is the depth-averaged kinematic viscosity, which can be expressed in terms of the Reynolds number Re (Lynden-Bell & Pringle 1974; Williams & Ferguson 1982), m is the mass column density above a certain physical depth, and Σ is the column density, which in the standard disk model is related to $\bar{w}$, $\dot{M}$, and R_1 as follows (for details see Hubeny 1989, 1990a, 1990b):

$$\Sigma = \frac{\dot{M}}{3\pi\bar{w}}\left[1-\left(\frac{R_1}{r}\right)^{1/2}\right]. \quad (4)$$

The presence of a depth-dependent viscosity, expressed by equation (2), causes internal energy generation, implying a nonconservative radiative flux in the atmosphere interior.

The structure equations plus the radiative transfer equation are solved self-consistently in local thermodynamic equilibrium (LTE) by the complete linearization method, using the universal code TLUSTY[1] (Hubeny 1988; Hubeny & Lanz 1995), which is able to compute stellar atmosphere as well as accretion disk models (in the past, a different variant called TLUSDISK [Kriz & Hubeny 1986; Hubeny 1990a, 1990b] was employed for the same problems, specifically dealing with disks). Following Diaz et al. (1996) only H, He, and continuum opacities were taken into account for the atmosphere structure calculation, along with free-particle processes and scattering. We also assumed that there was no radial radiative energy transfer and no disk irradiation by the BL or by the white dwarf.

Once the structure variables, like the temperature, density, and opacity, are calculated, the radiative transfer equation is solved again, including elements up to $Z = 30$, for all frequencies in the selected UV band. The specific intensities are calculated by the general spectral synthesis program SYNSPEC (Hubeny et al. 1994), taking into account the temperature, pressure, and density effects on opacity and line broadening. A set of spectra is assembled for a range of $\mu = \cos i$ values. The final integrated spectrum is the sum of all ring spectra corrected for Keplerian velocity and inclination (for more details see Diaz et al. 1996; Wade & Hubeny 1998).

Following others authors (e.g., Diaz et al. 1996; Diaz & Hubeny 1999; Long et al. 1994), $\zeta = \frac{2}{3}$ and Re = 5000 were used in this work as representative values. The resulting model spectra are not sensitive to these two parameters over a reasonable range of values. The internal radius of the disk was taken as equal to the WD radius, calculated with the mass-radius relation for carbon white dwarfs from Hamada & Salpeter (1961). Eight log-spaced rings were used for each disk model. This scale produces an appropriate sampling of the regions where the radial gradients are larger. The external radius was limited by two conditions: the last ring cannot have a temperature lower than 8000 K, or its radius cannot be larger than 0.7 times the primary Roche lobe radius. The former condition arises from the negligible contribution of the cooler regions in the UV. Those cool regions are possibly optically thin (Williams 1980). The latter condition is imposed by the tidal forces that disrupt the disk at larger radii (Osaki et al. 1993).

In order to estimate the WD contribution to the UV spectra of our sample, WD atmosphere model spectra were also calculated. These models consist of a hydrogen WD atmosphere with $\log g = 8$. The atmosphere structure was calculated with the TLUSTY code (Hubeny 1988; Hubeny & Lanz 1992), and its spectrum was synthesized using SYNSPEC (Hubeny et al. 1994).

3.2. *Multiparameter Optimization Method*

The optimization method used to constrain the parameters for each system is based on the generation of a grid of models in a three-dimensional space ($\dot{M}$, M_1, and i). The mass and inclination are first constrained by the most probable values found in the literature (Table 1). Thus, the M_1 and i intervals sweep a wide and suitable range for each parameter. These intervals are different for each system and depend on the parameter uncertainties. In order to cover a suitable volume in the parameter space, an M_1 minimum value of 0.4 $M_\odot$ was set. In the same sense, an inclination minimum value of 20° was used. For an initial guess of $\dot{M}$, the flux level of the observed spectrum is fitted by a simple blackbody accretion disk model (e.g., Wade 1984). The value calculated in this simple way is taken as a first guess for the disk atmosphere models. The $\dot{M}$ search interval ranges from 2 dex below that value to 2 dex above. In the case of the distance we are currently forced to fix values because of the degeneracy between the distance and disk model parameters. For each disk model a synthetic spectrum is calculated and compared with the observed one through the value of χ^2_{red}, calculated as follows:

$$\chi^2_{\mathrm{red}} = \frac{1}{l}\sum_{i=1}^{n}\frac{[y_i - y(\lambda_i)]^2}{\sigma_i^2}, \quad (5)$$

where l is the number of degrees of freedom, n is the number of the spectral elements, y_i is the value of the flux of the observed spectrum in the spectral element λ_i, $y(\lambda_i)$ is the flux value of the synthetic spectrum in the same spectral element, and σ_i is the observed spectrum's rms, estimated using a polynomial fit to the "line-free" continuum. All χ^2_{red} values in the three-dimensional space of the parameters were fitted by a smooth surface, and the

[1] See http://nova.astro.umd.edu.

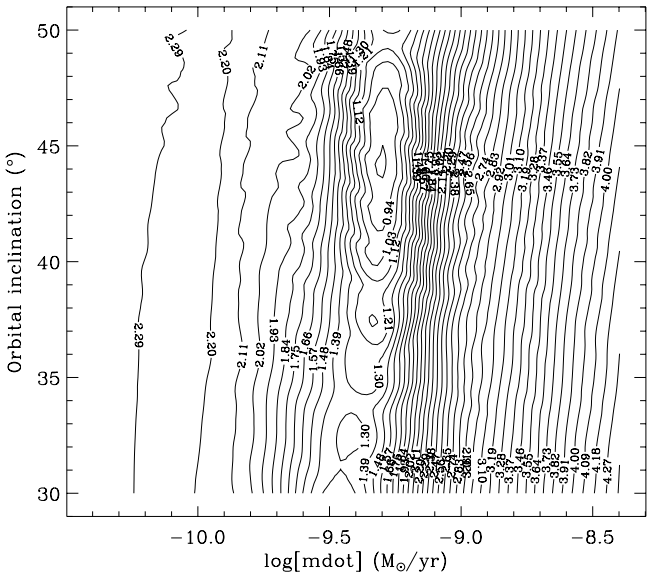

FIG. 1.—Sample of a log $\chi^2_{\rm red}$ surface for disk spectrum fitting. This sample corresponds to the fitting of the UV spectrum of KR Aur using $30^\circ < i < 50^\circ$, $-10.4 < \log\dot{M} < -8.4$, and $0.4\ M_\odot < M_1 < 0.8\ M_\odot$. A cut at $M_1 = 0.6\ M_\odot$ is shown

minimum $\chi^2_{\rm red}$ region was searched. The most probable $\dot{M}$ values for each system were those in the minimum $\chi^2_{\rm red}$ region, within the most probable values for the other parameters obtained from the literature. Figure 1 shows an example of one such surface, indicating the most probable parameter region.

A four-dimensional space was also used, including the distance as a free parameter. However, when distance was let free, in most cases the model did not converge to a bounded minimum $\chi^2_{\rm red}$ region, and it was impossible to fit the observed spectra within a reasonable four-dimensional parameter space ($\dot{M}$, M_1, i, and d). These fitting problems have already been found in earlier works (Wade 1988). In the present work these problems suggest that improvements are needed in the calculation of model spectra. This point is discussed in more detail in § 4.

The WD emission was not included as an additional free parameter; instead, the eventual contribution from a hot (40,000 K) WD was estimated for each object. We define disk-dominated CVs as those for which $\xi = f_{\rm WD}/f_{\rm disk} < 0.1$, where $f_{\rm WD}$ and $f_{\rm disk}$ are the integrated spectral flux from 1500 to 3250 Å for the WD and disk model, respectively.

4. RESULTS

4.1. *Model Behavior and Parameter Constraints*

4.1.1. *Analysis with Fixed Distance*

Using the method described in §§ 3.1 and 3.2, the $\chi^2_{\rm red}$ surfaces were analyzed at constant M_1 or i. Following this procedure, peculiar features, common behavior, and model families were identified in our sample of disks. Table 2 shows the search intervals used for each parameter for each system. When possible, the parameter region was bounded within the errors found in the literature (Table 1). Table 2 also shows the calculated values for $\dot{M}$ in $M_\odot\ {\rm yr}^{-1}$, and its dex error. The observed equivalent widths of the C IV (λ1550) and He II (λ1640) emission lines were also measured.

A characteristic shape is seen in all $\chi^2_{\rm red}$ surfaces. They show a deep depression with the form of a narrow band (Fig. 1). This band basically corresponds to disk models that are able to reproduce the observed flux level (with that fixed distance). The quality of the model fit to the observed continuum shape is described by the details within the band (see Fig. 1). It was also found that the band topology depends on the orbital inclination when we cut the three-dimensional space at a fixed M_1. For systems with low inclination, the band is almost a straight vertical valley, with a small tilt toward higher accretion rate values. This is caused mainly by effect of the aspect factor cos i on the flux value. A decrement of this factor is roughly compensated for by a corresponding increment in the accretion rate. For systems with high orbital inclination we find that the band shape changes to a bent one, with a slope decreasing toward higher accretion rates and higher orbital inclinations. This effect is caused by the combined action of the steep cos i factor change and limb darkening. In most systems with low inclination, the $\chi^2_{\rm red}$ valley depth is almost constant, but for systems with high inclination, the bottom tends to sink for larger values of the inclination or to form a small local minimum around some particular inclination point. The minimum band at a fixed inclination value is not absolute; i.e., for different values of M_1, such a minimum migrates. As expected, for larger M_1 values the band moves toward lower values of $\dot{M}$, and an eventual minimum moves to higher orbital inclinations. This happens due to the combined action of the three parameters to maintain the flux level and color. It is found that the $\chi^2_{\rm red}$ value decreases for cooler disks (i.e., lower values for M_1 and $\dot{M}$ [eq. (1)]) but does not always achieve an absolute minimum value in the three-dimensional space (M_1, $\dot{M}$, and i). This behavior indicates that the disk models used here, in most cases, generate spectra that are too blue in comparison with the observed data. This problem, which has already been found using classical atmosphere models, may suggest that extra sources of continuum light are possibly being neglected and/or that the radial temperature law is not correct. This is the reason why it is not possible to adjust these three parameters (M_1, $\dot{M}$, and i) simultaneously without constraints. As an example, values of i and M_1 were limited in order to constrain the $\dot{M}$ values.

After performing the analysis, we have convinced ourselves that the absolute $\chi^2_{\rm red}$ values lack statistical meaning in this context. Therefore, $\chi^2_{\rm red}$ was used to compare models only. Their numerical values are high because of at least two effects: (1) The uncertainty per resolution element is estimated from the residuals of a low-order fit to selected line-free continuum regions. Unfortunately, these regions also contain lines which do not behave like noise. An average residual (rms) is used as $\sigma(\lambda)$ in the $\chi^2_{\rm red}$ calculation. The rms is in fact different from the pure noise $\sigma(\lambda)$ value at each wavelength. (2) As pointed out in the discussion, the model spectra are not capable of describing the line profiles and intensities. On the other hand, in many cases the model spectra contain lines that do not appear in the observations, thus increasing $\chi^2_{\rm red}$. The description of the upper disk atmosphere was found to be oversimplified or inaccurate, but there are also expected differences in the actual chemical abundances and effective gravities.

Using the calculated $\dot{M}$ values for the target sample, we have performed a search for its correlation with other system parameters. Figure 2 shows the accretion rate as a function of the orbital period. In contrast with the well-defined correlation derived by Patterson (1984), a higher dispersion in the $\dot{M}$-$P_{\rm orb}$ diagram is found. The values are also systematically higher than those calculated by Patterson and more in agreement with those calculated by Rutten et al. (1992). The weak correlation between $\dot{M}$ and $P_{\rm orb}$ found in this work is expressed by equation (6). This relation is less steep than the classical Patterson relation. These features are mostly due to the special sample chosen for the present work, which is limited to high accretion rate systems with bright disks. Another correlation revisited was that between the absolute magnitude M_V and the accretion rate. The absolute magnitudes corrected for inclination effects and limb darkening were calculated

TABLE 2

ACCRETION MASS RATES CALCULATED FOR 33 CVs USING THE ATMOSPHERE DISK MODEL AND A FIXED DISTANCE

Object	P_{orb} (days)	M_1 Range ($M_\odot$)	i Range (deg)	Distance (pc)	$\dot{M}$(BB) ($M_\odot$ yr^{-1})	log $\dot{M}$ ($M_\odot$ yr^{-1})	ξ	η
CP Pup	0.06	0.5–0.9	20–40	700	2.29×10^{-9}	−8.74(23)	0.02	0.79
BK Lyn	0.07	0.25–0.7	20–45	150	3.29×10^{-10}	−9.75(18)	4.86	0.54
V592 Cas	0.12	0.9–1.3	15–40	330	7.35×10^{-9}	−8.20(20)	0.02	0.86
V442 Oph	0.12	0.3–0.7	50–80	130	3.13×10^{-9}	−8.51(55)	0.21	0.99
DN Gem	0.13	0.8–1.2	30–60	1600	4.11×10^{-9}	−8.72(39)	0.02	0.46
SW Sex	0.13	0.4–0.8	62–82	450	4.23×10^{-9}	−8.75(25)	0.10	0.42
DW UMa	0.14	0.5–1.0	65–85	930	1.40×10^{-8}	−8.14(18)	0.05	0.52
V603 Aql	0.14	1.0–1.4	5–25	235	2.10×10^{-9}	−8.85(16)	0.02	0.67
V1315 Aql	0.14	0.5–0.9	75–85	300	1.24×10^{-9}	−8.90(62)	0.42	1.02
RR Pic	0.15	0.75–1.15	55–75	250	6.68×10^{-9}	−8.27(40)	0.02	0.80
PX And	0.15	0.5–0.9	64–84	200	2.56×10^{-10}	−9.52(20)	0.98	1.18
V533 Her	0.15	0.75–1.15	55–75	1200	1.25×10^{-8}	−8.05(15)	0.01	0.71
V794 Aql[a]	0.15	0.8–1.2	25–55	200	8.84×10^{-11}	−10.29(38)	1.39	0.58
LX Ser	0.16	0.3–0.7	70–85	340	1.37×10^{-9}	−8.70(30)	0.44	1.46
CM Del	0.16	0.3–0.7	60–85	280	9.42×10^{-9}	−8.38(43)	0.10	0.44
KR Aur	0.16	0.4–0.8	30–50	180	4.83×10^{-10}	−9.35(29)	0.20	0.92
IX Vel	0.19	0.7–1.0	45–70	95	1.00×10^{-8}	−8.16(20)	0.02	0.69
UX UMa	0.2	0.4–0.8	60–80	340	1.69×10^{-8}	−7.85(15)	0.02	0.84
T Aur	0.2	0.5–0.9	50–70	960	3.10×10^{-8}	−7.64(25)	0.01	0.74
HR Del	0.21	0.5–0.9	30–50	285	1.46×10^{-8}	−7.99(25)	0.01	0.70
V3885 Sgr	0.22	0.6–1.0	30–50	195	1.31×10^{-8}	−8.03(39)	0.01	0.71
V347 Pup	0.23	0.5–0.8	65–85	510	1.05×10^{-8}	−8.22(26)	0.06	0.57
VY Scl	0.23	1.0–1.4	20–40	500	6.19×10^{-9}	−8.28(31)	0.01	0.85
RW Tri	0.23	0.4–0.8	60–80	345	6.17×10^{-9}	−8.33(25)	0.05	0.76
RW Sex	0.25	0.7–1.1	25–45	290	1.25×10^{-8}	−8.00(20)	0.01	0.80
TW Pic[b]	0.27	0.5–0.9	25–26	720	3.08×10^{-9}	−8.65(32)	0.02	0.73
AC Cnc	0.3	0.5–1.0	60–80	550	1.17×10^{-9}	−9.02(29)	0.16	0.82
V363 Aur	0.32	0.7–1.1	60–80	650	5.72×10^{-9}	−8.34(17)	0.03	0.80
BT Mon	0.33	0.8–1.2	65–84	1700	4.24×10^{-8}	−7.71(33)	0.02	0.46
RZ Gru	0.36	0.8–1.2	10–35	440	2.42×10^{-9}	−8.71(26)	0.02	0.81
QU Car	0.45	0.8–1.2	35–65	500	1.19×10^{-7}	−7.26(32)	0.00	0.46
DI Lac	0.54	0.5–1.0	5–30	1318	8.01×10^{-8}	−7.22(12)	0.00	0.75
V841 Oph[b]	0.6	1.0–1.4	30–70	255	1.21×10^{-9}	−9.03(45)	0.02	0.77

NOTES.—The blackbody disk $\dot{M}$ value and the ranges in M_1 and i used in the fitting are shown, as well as the adopted distance. Also shown is the ratio between a 40,000 K WD flux and a disk flux in the UV (ξ) (see text) and the ratio between the $\dot{M}$ values calculated with the atmosphere disk model and the BB approach (η).

[a] Values calculated using the *HST* STIS spectrum in the high state.

[b] Lower limit for $\dot{M}$ due to an upper limit on M_1.

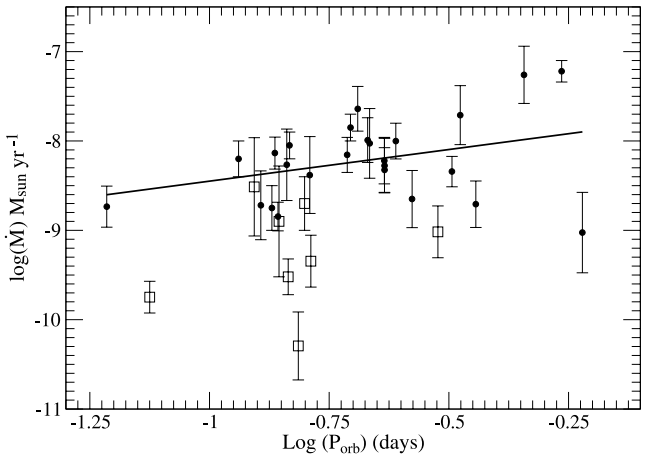

FIG. 2.—Dependence of the mass accretion rate $\dot{M}$ (calculated using fixed distances) on orbital period for quiescent nova and nova-like CVs. The best linear fit is shown and is expressed by eq. (6). The circles show disk-dominated CVs, while the squares represent objects with an eventual contribution from the WD. The latter were not considered in the linear fit.

using the Warner (1986) approximation. As expected, the M_V values show a strong correlation with $\dot{M}$ (Fig. 3). A simple linear fit leads to equation (7):

$$\dot{M} = 1.82^{+1.64}_{-0.86} \times 10^{-8} P_{\rm orb}^{0.7\pm0.40}\ M_\odot\ {\rm yr}^{-1}, \quad (6)$$

$$\dot{M} = 1.69^{+1.26}_{-0.71} \times 10^{(-0.34\pm0.05)M_V - 7}\ M_\odot\ {\rm yr}^{-1}. \quad (7)$$

Both equations (6) and (7) were derived using the disk-dominated subsample, and their correlation coefficients are 0.37 and 0.78, respectively.

For completeness and comparison, the values calculated with blackbody standard disk models were also included in Table 2. The computed blackbody fluxes were corrected for limb darkening in first order using the Eddington approximation (e.g., Paczyński & Schwarzenberg-Czerny 1980). The ratio η between these values and the atmosphere disk results was also calculated. On average, the disk atmosphere models reveal slightly lower mass transfer rates when compared to limb-darkened blackbody disks (∼75%). However, individual disk models can be very different, depending on the particular observed continuum shape. Due to limb darkening the continuum is formed in higher and cooler regions in the disk

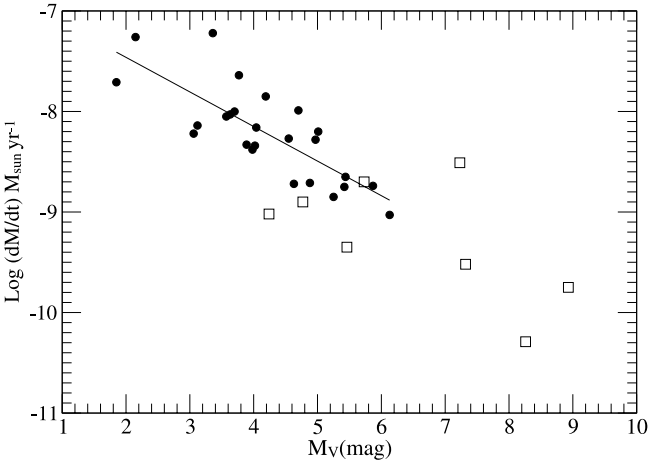

FIG. 3.—Dependence of accretion mass rate $\dot{M}$ (calculated using fixed distances) on the absolute magnitude of the disk M_V(disk) corrected for inclination effects. The best linear fit is shown and is given by eq. (7). The circles show disk-dominated CVs, while the squares represent objects that may show an eventual contribution from the WD. The squares were not considered in the linear fit.

atmosphere, and thus produces a less intense and redder observed spectrum, which can also be interpreted as a lower $\dot{M}$ if the limb darkening is not taken into account.

4.1.2. *Analysis with Variable Distance*

The distance was scaled as a free parameter for each model in the grid to values that allowed the matching of the observed flux level. The calculated $\chi^2_{\rm red}$ values were then analyzed in a four-dimensional space (M_1, $\dot{M}$, i, and d) in order to search for an absolute minimum. For most cases this search was not successful. The common behavior of the $\chi^2_{\rm red}$ slices leads to a simple conclusion: there is not a unique set of parameters capable of fitting the UV spectra within the parameter frame using this disk model. The synthetic spectra are too blue, and the models improve toward cooler or more inclined disks without achieving a minimum. Nevertheless, we found a few systems where there is a reasonably well defined $\chi^2_{\rm red}$ minimum region. In some cases the minimum $\chi^2_{\rm red}$ parameters are far from those found in the literature. In particular, inconsistent values for the distance are inferred. In addition, the

TABLE 3

BEST SOLUTIONS FOUND USING FREE SCALING OF DISTANCE

Object	$\dot{M}$ ($M_\odot$ yr^{-1})	M_1 ($M_\odot$)	i (deg)	d (pc)	$d_{\rm lit}$[a] (pc)
V592 Cas	7.08×10^{-10}	0.95	40	130	330
V442 Oph	6.00×10^{-9}	0.4	67	130	130
CM Del	2.00×10^{-9}	0.65	82	147	215

[a] Mean distance from the literature for comparison.

$\chi^2_{\rm red}$ minimum regions are actually open regions, similar to the bands found in the fixed-distance case (Fig. 4). In fact, as already seen in the previous section, this feature is caused by the degeneracy between parameters that arises when one tries to describe only the continuum shape.

Due to the noise in the observed spectra, and the inability of the current model to describe the emission lines, many significant spectral features cannot be used to constrain the models. This leads to the strong degeneracy among the parameters within this disk model. Figure 4 shows two examples of $\chi^2_{\rm red}$ surfaces with free distance scaling for CM Del. This figure shows that the region of minimum $\chi^2_{\rm red}$ values is very close to the high-inclination limit, $\sim 85^\circ$, with $\log \dot{M}$ between -9 and -8.7 and $M_1 \sim 0.6$–$0.7\ M_\odot$. For this particular fit, the spectrum had to be scaled to a distance of only 147 pc. That distance is still reasonable when compared to the values found in the literature. But in most cases the distance for which the spectrum has to be scaled is too low in comparison with the literature values. On the other hand, the M_1 values are systematically smaller than the values from other studies. Only for three cases was a reasonable set of parameters obtained using the free-distance method: the nova-like systems V442 Oph, CM Del, and V592 Cas. Table 3 shows the best-fit parameter values, including the distance. For most of the systems it was impossible to find a reduced parameter space when the distance was left as an unconstrained parameter.

4.1.3. *The WD Contribution*

For every system the ratio $\xi = f_{\rm WD}/f_{\rm disk}$ was calculated using the WD model described in § 3.2. The results are shown in the last

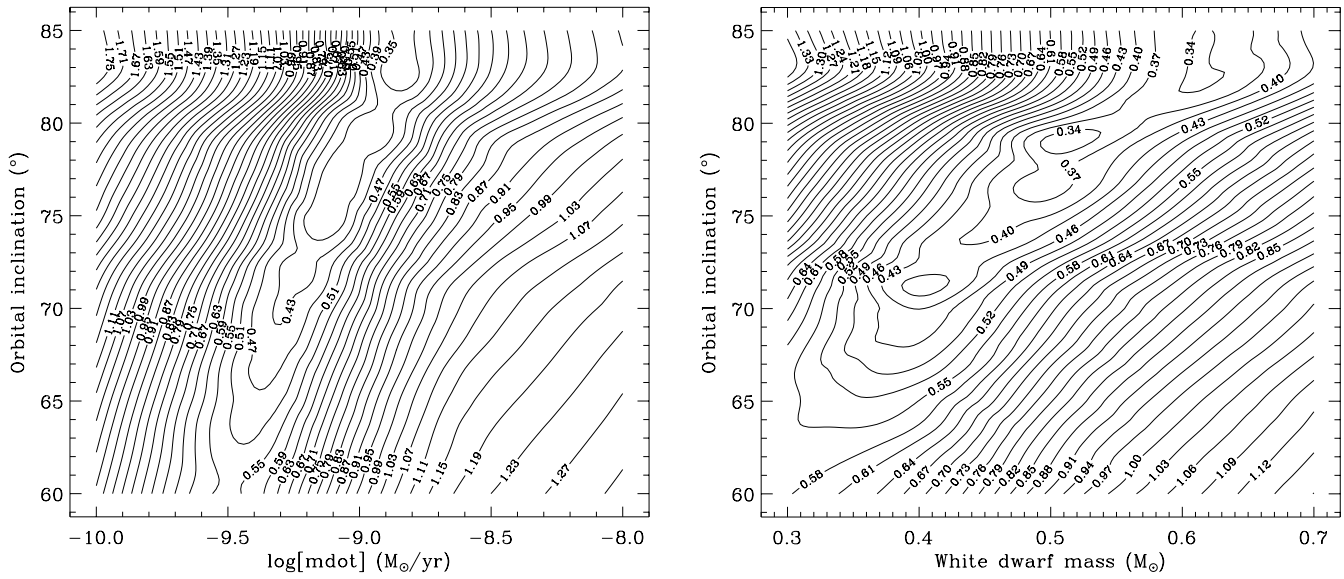

FIG. 4.—Log $\chi^2_{\rm red}$ surfaces for the spectral fit of CM Del. A free scaling of distance was employed. *Left*, Cut of the three-dimensional parameter space at $M_1 = 0.7\ M_\odot$; *right*, cut at $\log \dot{M} = -8.66\ M_\odot$ yr^{-1}.

column in Table 2. It is easy to see that in most cases even a hot (40,000 K) WD does not contribute considerably in the UV in such a high-$\dot{M}$ sample. But there are cases (10 nova-like systems) for which an eventual contribution of a hot WD should not be ignored. Systems with an eventual contribution of the WD belong to the SW and VY nova-like subclasses (V442 Oph, V1315 Aql, PX And, LX Ser, KR Aur, V794 Aql, and AC Cnc). The latter subtype of CV presents variability and sporadic low states. This could be caused by a spontaneous decrease in the accretion rate in the disk, which could unveil the white dwarf (e.g., Knigge et al. 2000, 2004). Interestingly, BK Lyn is a UX-type nova-like system (Ritter & Kolb 2003),[2] and its ξ-value was found to be 0.16.

4.2. *Discussion*

4.2.1. *Disk Stability*

Systems with no record of dwarf nova activity, like the systems in our sample, should maintain a relatively high mass transfer rate, above the critical mass transfer rate for disk instability outbursts. In that sense the mass transfer rates derived using the disk atmosphere models are consistent with the absence of dwarf nova–type outbursts in recent broadband photometry of our targets. The disk instability model predicts that the critical local mass transfer rate is a function of radius and M_1, with a weak dependence on the α viscosity parameter (e.g., Lasota 2001). If the disk is stable at the outer parts, it should be stable as a whole. Figure 5 shows that virtually all analyzed disks are above the stability curve.

It is important to take into account the influence of the parameter errors on that conclusion. Any change in the parameters that would modify the flux level or color would produce a change in $\dot{M}$ that could put the system in the instability zone. For example, the distance is one of the most inexact parameters; a lower value of distance would produce a lower value of $\dot{M}$, and some systems could fall into the instability zone. The adopted disk radius definition would also influence the present instability analysis. If the disk is larger, then the minimum $\dot{M}$ for stability increases and could eventually reach our $\dot{M}$ values. In this case we also should consider that the relation used to calculate the instability curves in Figure 5 does not take into account the influence of the hot spot and irradiation on the critical $\dot{M}$. Both effects lower that value, which tends to assure the stability of most of the disks in the sample. Considering the errors in $\dot{M}$, some systems may be close to the instability limit (e.g., V794 Aql, DN Gem, V442 Oph, and V1315 Aql). At least two of these systems are known to have VY Scl–type low states. During the mass transfer decrease toward their low states they would certainly be found below the critical mass transfer curve, according to our simulations. Hameury & Lasota (2002) have proposed an explanation for the absence of disk instabilities during such reduced mass transfer events on the basis of the presence of magnetic white dwarfs in these systems, with magnetic moments comparable to those found in intermediate polars.

4.2.2. *Comments on Peculiar Systems*

We have found some intriguing peculiarities in a few objects of our sample. For example, the BT Mon spectra could not be even roughly modeled by any set of parameters. All models are far too blue. The models for TW Pic are also too blue. This system shows strong emission lines and has a low orbital inclination; this behavior may suggest an error in the inclination determination or an optically thin disk. Opposing that, for T Aur every model generated within parameter range is too red, unlike what happened with most of the disks in the sample. It may suggest an error in the $E(B-V)$ estimation.

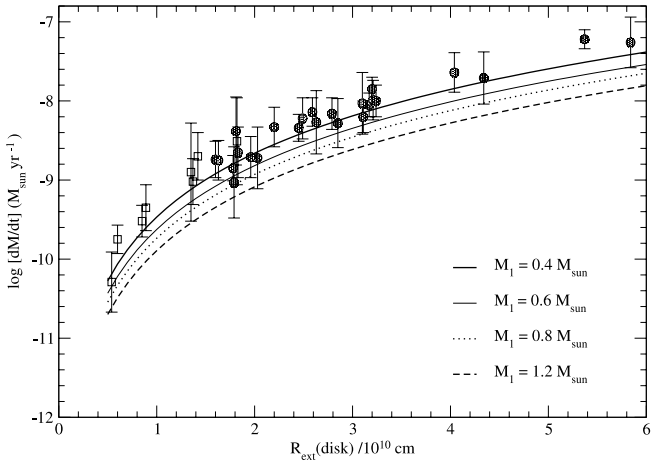

FIG. 5.—Mass transfer rate as a function of disk radius for all disks in the sample. The curved lines correspond to the critical $\dot{M}$ for stable mass transfer, considering white dwarf masses ranging from 0.4 to 1.2 $M_\odot$. The circles correspond to disk-dominated CVs, while there may be some contribution from the white dwarf to the UV emission in the systems plotted with squares (see text).

There is no way to fit the observed spectra of BK Lyn with this accretion disk model; every model computed has a weak flux level or a too-red continuum. Considering the M_1 value, the flux level, the strong emission lines, and the low orbital inclination, it is possible that this system has an optically thin disk with a very low accretion rate.

V794 Aql presents strong emission lines in both spectra collected for this work: the low state (*IUE*) and also the high state (STIS). Other spectra taken with *IUE* in 1994 show V794 Aql in an even higher state and show emission lines weaker than previous spectra. Apparently this is a noneclipsing system, which would discard the explanation of a flat continuum and emission lines caused by high inclination. Its variability and the spectrum appearance suggest an unstable and optically thin disk (Honeycutt et al. 1994). In addition, the $\dot{M}$ calculated here seems too low for a system above the period gap.

We could not find any estimates of M_1 and i for RZ Gru, but because of the deep P Cygni profiles we suspect that this system has a low orbital inclination. The WD mass assumed for this work is 1 $M_\odot$. Due to these unconstrained values, the calculated $\dot{M}$ values have a considerable uncertainty.

The distance used for DI Lac is 1300 pc; this value was calculated using the M_V value from Warner (1987). Moyer et al. (2003), using the *HST* STIS spectrum, fitted the same atmosphere disk model, but their best model leads to a distance of ~2000–2500 pc. Nevertheless, by using the same spectrum and disk model, we found that such estimates for the distance seem incompatible with their values for the accretion rate.

4.2.3. *Comments on the Disk Model Spectra*

The simulations presented in this work indicate that the current generation of accretion disk models cannot yet reproduce completely the spectrum shape of CVs in the UV. It was shown that in this disk model we still find a flux/color dichotomy. This effect has been found already by Wade (1988), who used concentric rings of classical stellar atmospheres. He concluded that the models that could match the continuum shape appear to be $\dot{M} \sim 2$ dex below the models that could match the flux level.

In our study we left $\dot{M}$, M_1, and i free within suitable intervals and constrained d to a fixed value. In this case we still found that

[2] For an updated version see RKcat7.6.

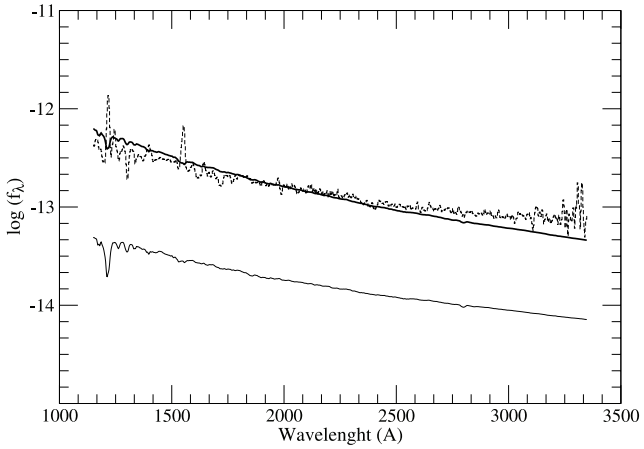

FIG. 6.—*IUE* UV spectrum of UX UMa (*dotted line*), the atmosphere disk model spectrum that best fit the flux level (*thick solid line*), and the atmosphere disk model that best fit the continuum shape (*thin solid line*). The former model was calculated with $M_1 = 0.8\,M_\odot$, $\dot{M} = 1.51 \times 10^{-8}\,M_\odot\ \mathrm{yr}^{-1}$, and $i = 78^\circ$, while the latter was calculated with $M_1 = 0.4\ M_\odot$, $\dot{M} = 5.49 \times 10^{-9}\ M_\odot\ \mathrm{yr}^{-1}$, and $i = 80^\circ$.

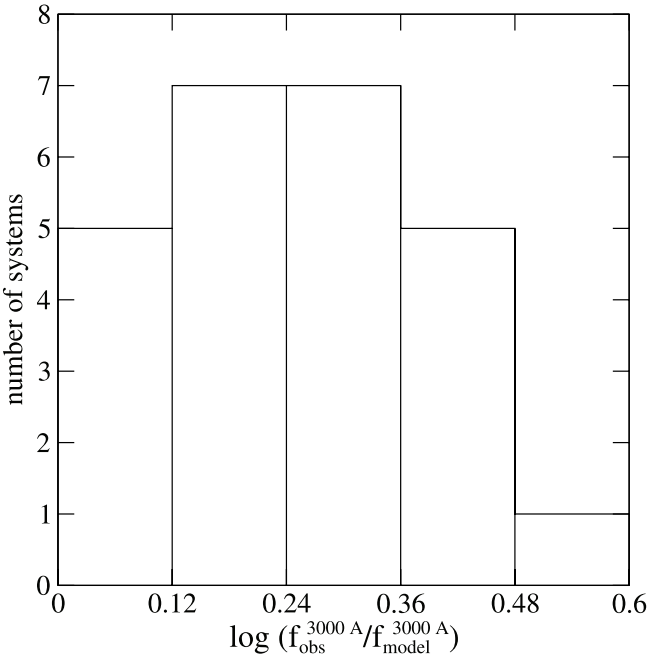

FIG. 7.—Distribution of the color/flux dichotomy in the disk-dominated subsample. The dichotomy is evaluated as $\log\,[f_{\mathrm{obs}}(3000\ \text{Å})/f_{\mathrm{model}}(3000\ \text{Å})]$, with the model and the observed fluxes matched at 1480 Å.

the best models are too blue. Figure 6 shows the *IUE* spectrum of UX UMa together with the model that matches the flux level and the model that matches the color. The former is bluer than the observed spectrum by a factor of $\sim$2, and the second is $\sim$10 times dimmer in flux level. On the other hand, there are systems (a few of them) for which the dichotomy is small, for instance, in the fit of the V442 Oph spectra. In order to evaluate quantitatively that dichotomy in our sample, the model that reproduces the flux level was matched to the observed spectrum at 1480 Å, and the flux ratio at 3000 Å was measured for each system. The histogram in Figure 7 shows how that ratio, calculated as $\log\,(f_{\mathrm{obs}}^{3000}/f_{\mathrm{model}}^{3000})$, is distributed in the sample. There is a high dispersion of values peaking close to the average at $\sim$0.3 dex. These values are not much different from those found by Wade (1988). This can be explained if we realize that the disk atmosphere structure still resembles a stellar atmosphere because the dissipation of viscous energy occurs at high optical depths. Even for small ζ-values the outer layers in the atmosphere only transport the energy generated at the inner region. A similar situation happens in a stellar atmosphere. A viscosity law with a very small ζ-value will produce energy at more superficial layers. This leads to increased viscosity and dissipation in low-density regions, which in its turn, without a consistent model of dissipation in those conditions, will bring convergence and instability problems within a local thermodynamic equilibrium framework (Shaviv & Wehrse 1986; Hubeny 1990a, 1990b).

One possible path to improving the fits to the data in the context of the disk models would be to adjust the place in the atmosphere where the dissipation of viscous energy occurs, increasing the amount of dissipation in the upper atmosphere. This, however, is beyond the scope of the present work.

An important factor affecting the spectrum shape is the adopted radial temperature law (eq. [1]). A good alternative to repair the flux/color problem could be the use of a nonstandard law. Different temperature laws have been studied (Orosz & Wade 2003), and it has been shown that a less steep law better reproduces the observed spectra. But the physical mechanism responsible for flattening the temperature profile is not yet well known It is possible that a different temperature law is caused by mass loss in a wind (e.g., Knigge 1999) or disk irradiation by the BL. However, there are observational constraints available for guiding experiments with new radial temperature distributions. Eclipse-mapping results suggest that the radial temperature profiles are not too different from the standard $T \propto R^{-3/4}$ law (e.g., Rutten et al. 1992; Linnell et al. 2007). The importance of including an extended optically thin component in the accretion disk model is evident from the strong emission lines and the P Cygni profiles observed in the UV spectra. The P Cygni profiles, especially for C IV and N V, present a deep absorption component with minimum flux at relatively low velocities when compared to OB stars (e.g., Córdova & Howarth 1987). The correlation between the equivalent width of the emission lines and the orbital inclination was confirmed, and, in addition, it was found that systems with low $\dot{M}$ do not show strong emission lines. This underlines the close relation between the disk model and the emission-line flux, which shows the need to include an extended optically thin region in the next generation of models.

As already mentioned, the degeneracy present in the solutions is due to a strong correlation among the variables within the model. Also, there are too many parameters to be fit (M_1, $\dot{M}$, i, and eventually d), considering that mostly the continuum shape and level are analyzed. Furthermore, the other unknown parameters, $E(B-V)$, ζ, and Re, were kept fixed. Unlike $E(B-V)$, however, it can be shown that the variation of those last two quantities does not strongly affect the spectrum appearance. It is important to remember that, due to the degeneracies between the parameters, the values calculated here strongly depend on each other. In other words, in order to calculate $\dot{M}$ we were forced to limit the values of the rest of parameters (M_1 and i) within the literature values.

Two degrees of correlation exist among the parameters. A stronger correlation exists between M_1 and $\dot{M}$, and a weaker correlation between these quantities and the orbital inclination. These correlations come from the disk model itself, as much as from the atmosphere structure and spectral synthesis. These correlations are linked to the standard effective temperature distribution (eq. [1]) used as boundary condition for the atmosphere structure. Because of the dependence of the radial profile on M_1 and $\dot{M}$ (taking into account the mass-radius relation for the WD), it is difficult to uncouple these parameters, since the reddening caused by a smaller M_1 can be compensated for by a higher accretion rate. A weaker

correlation between M_1 and i or between $\dot{M}$ and i is evident from Figure 4, unlike what happens in the (M_1, $\dot{M}$)-plane, where the depth of the valley is almost constant. Limb darkening could be the main cause of such weak uncoupling between those parameters, since it strongly depends on the orbital inclination. However, since the changes of concavity in the continuum shape are too small and the observed spectral noise is high, it is difficult to disentangle those parameters completely. If the accretion disk model included the necessary physics to describe the emission-line profiles and the optically thin emission in the continuum, we could eventually break down those degeneracies.

In a different analysis, the distance d was left completely free, being scaled in order to match the spectrum level. A search for a complete set of parameters that could fit the spectra was performed for the whole sample. However, this search was successful for only a few systems, and within this subset, in only three cases were the parameters derived comparable to those found in previous works. These differences appear in a different degree for every system.

5. SUMMARY AND CONCLUSIONS

A sample of 33 CVs with stable disks (nova-like systems and old classical novae) was selected in order to test the current generation of accretion disk models. In addition, using this model, the accretion rate for each system in the sample was estimated. A graphical multiparametric optimization method was used to verify how model spectra reproduce the observed spectra in the UV. A grid of disk models was calculated for each system, sweeping a three-dimensional space of parameters (M_1, $\dot{M}$, and i) and maintaining a fixed or free distance. The minimum $\chi^2_{\rm red}$ regions within that space selected the model properties and constrained the possible values of $\dot{M}$.

Almost all models are too blue when compared with the observed spectra. The models calculated using a free scaling distance can also be accommodated toward the reddest possible continua and faint disks. Strong degeneracies among system parameters were found in the solutions for each system. The current generation of accretion model spectra cannot reproduce in detail the observed absorption-line profiles, which would be helpful for breaking those degeneracies and achieving a description of UV spectra with a unique set of parameters. In fact, the emission-line fluxes appear strongly coupled to other disk properties, due to their correlation with the orbital inclination and accretion rate. We also found that the disk atmosphere model used here, even considering that it is more sophisticated, presents some problems already noted in previous works, like the flux/color dichotomy.

These findings point toward the need to improve the disk model by incorporating a component from an extended optically thin region, which can be contributed by a wind and/or a chromosphere. In that case, it will not be possible to use the local thermodynamic equilibrium approach. Disk irradiation by the boundary layer or by the central star, and nonstandard temperature profiles, would help to improve the model behavior. An additional possibility here is to consider a truncation or evaporation of the inner disk (as also suggested by Long et al. [1994] on observational grounds and by Liu et al. [1997] on theoretical grounds). Another possibility is to modify the viscosity law (eq. [2]) with some additional physical insight, for instance by using constraints on the viscosity following from numerical simulations of the magneto-rotational instability (Balbus & Hawley 1991).

Excluding those systems for which a hot white dwarf may influence the UV continuum, the average of $\dot{M}$ for the whole sample of disk-dominated CVs is $\sim 1.1 \times 10^{-8}\ M_\odot\ {\rm yr}^{-1}$, while for nova-like systems (15 systems) it is $\sim 9.3 \times 10^{-9}\ M_\odot\ {\rm yr}^{-1}$, and for quiescent novae $\sim 1.3 \times 10^{-8}\ M_\odot\ {\rm yr}^{-1}$. According to our $\dot{M}$ values, all disks were found in a stable mass transfer regime. The atmosphere disk model structure has a crucial role in estimating $\dot{M}$, and limb darkening is significant in high-inclination systems. It is important to continue the search for improvements on disk spectral synthesis, aiming at a better understanding of the physics of viscosity and emission-line-production mechanisms in accretion disks.

We thank the financial support from CAPES, CNPq (process 143070/2005-3), and FAPESP (process 2005/04128-5). M. P. D. acknowledges the support from CNPq under grant 301029. We are thankful to Jorge Horvath for carefully reading this manuscript. We also thank the anonymous referee for his valuable comments.

REFERENCES

Araujo-Betancor, S., et al. 2003, ApJ, 583, 437
Balbus, S. A., & Hawley, J. F. 1991, ApJ, 376, 214
Baptista, R., Steiner, J. E., & Horne, K. 1996, MNRAS, 282, 99
Barret, P. 1996, PASP, 108, 412
Berriman, G., Szkody, P., & Capps, R. W. 1985, MNRAS, 217, 327
Bruch, A., & Engel, A. 1994, A&AS, 104, 79
Buckley, D. A. H., & Tuohy, I. R. 1990, ApJ, 349, 296
Cardelli, J. A., Clayton, G. C., & Mathis, J. S. 1989, ApJ, 345, 245
Córdova, F. A., & Howarth, I. D. 1987, in Scientific Accomplishments of the *IUE*, ed. Y. Kondo (Dordrecht: Reidel), 467
Diaz, M. P., & Bruch, A. 1997, A&A, 322, 807
Diaz, M. P., & Hubeny, I. 1999, ApJ, 523, 786
Diaz, M. P., & Ribeiro, F. 2003, AJ, 125, 3359
Diaz, M. P., Wade, R., & Hubeny, I. 1996, ApJ, 459, 236
Dobrzycka, D., & Howell, S. 1992, ApJ, 388, 614
Downes, R., & Duerbeck, H. 2000, AJ, 120, 2007
Duerbeck, H. W. 1999, Inf. Bull. Variable Stars, 4731, 1
Engle, S. G., & Sion, E. M. 2005, PASP, 117, 1230
Eracleous, M., Halpern, J., & Patterson, J. 1991, ApJ, 382, 290
Froming, C. Long, K. S., & Baptista, R. 2003, AJ, 126, 964
Godon, P., Seward, L., Sion, E. M., & Szkody, P. 2006, AJ, 131, 2634
Greenstein, J. L., & Oke, J. B. 1982, ApJ, 258, 209
Greiner, J. 1998, A&A, 336, 626
Hamada, T., & Salpeter, E. 1961, ApJ, 134, 683
Hameury, J. M., & Lasota, J. P. 2002, A&A, 394, 231
Hamilton, R. T., & Sion, R. M. 2004, PASP, 116, 926
Hoard, D. W., & Szkody, P. 1996, ApJ, 470, 1052
Hoard, D. W., & Szkody, P. 1997, ApJ, 481, 433
Honeycutt, R. K., Cannizzo, J. K., & Robertson, J. W. 1994, ApJ, 425, 835
Howell, S. B., Lorne, N. A., & Rappaport, S. 2001, ApJ, 550, 897
Hubeny, I. 1988, Comput. Phys. Commun., 52, 103
———. 1989, in Theory of Accretion Disks, ed. F. Meyer et al. (Dordrecht: Kluwer), 445
———. 1990a, ApJ, 351, 632
———. 1990b, in IAU Colloq. 129, Structure and Emission Properties of Accretion Disks, ed. E. Bertout et al. (Gif-sur-Yvette: Editions Frontières), 227
Hubeny, I., & Lanz, T. 1992, A&A, 262, 501
———. 1995, ApJ, 439, 875
Hubeny, I., Lanz, T., & Jeffery, C. S. 1994, St. Andrew Univ. Newsl. Anal. Astron. Spectra, 20, 30
Huber, M. E., Howell, S. B., Ciardi, D. R., & Fried, R. 1998, PASP, 110, 784
Hunger, K., Heber, U., & Koester, D. 1985, A&A, 149, L4
King, A. 1996, Ap&SS, 237, 169
Knigge, C. 1999, MNRAS, 309, 409
Knigge, C., Araujo-Betancor, S., Gänsicke, B. T., Long, K. S., Szkody, P., Hynes, R. I., Hoard, D. W., & Dhillon, V. S. 2004, ApJ, 615, L129
Knigge, C., Long, S., Hoard, D. W., Szkody, P., & Dhillon, V. S. 2000, ApJ, 539, L49
Ko, Y., Lee, Y. P., Schlegel, E. M., & Kallman, T. R. 1996, ApJ, 457, 363
Kriz, S., & Hubeny, I. 1986, Bull. Astron. Inst. Czechoslovakia, 37, 129
Kurucz, R. L. 1979, ApJS, 40, 1
La Dous, C. 1989, A&A, 211, 131
Lasota, J. P. 2001, NewA Rev., 45, 449

Linnell, A. P., Godon, P., Hubeny, I., Sion, E. M., & Szkody, P. 2007, ApJ, 662, 1204
Liu, B. F., Meyer, F., & Meyer-Hofmeister, E. 1997, A&A, 328, 247
Long, K. S., Wade, R. A., Blair, W. P., Davidsen, A. F., & Hubeny, I. 1994, ApJ, 426, 704
Lynden-Bell, D. 1969, Nature, 223, 690
Lynden-Bell, D., & Pringle, J. E. 1974, MNRAS, 168, 603
McArthur, B. E., et al. 1999, ApJ, 520, L59
Meliani, M. T., de Araujo, J. C. N., & Aguiar, O. D. 2000, A&A, 358, 417
Mouchet, M., Bonnet-Bidaud, J. M., Buckley, D. A., & Tuohy, I. R. 1991, A&A, 250, 99
Moyer, E., Sion, E. M., Szkody, P., Gänsicke, B., Howell, S., & Starrfield, S. 2003, AJ, 125, 288
Nadalin, I., & Sion, E. M. 2001, PASP, 113, 829
Orosz, J. A., & Wade, R. 2003, ApJ, 593, 1032
Osaki, Y., Hirose, M., & Ichikawa, S. 1993, in Accretion Disks in Compact Stellar Systems, ed. J. C. Wheeler (Singapore: World Sci.), 272
Paczyński, B., & Schwarzenberg-Czerny, A. 1980, Acta Astron., 30, 127
Patterson, J. 1984, ApJS, 54, 443
Patterson, J., & Raymond, J. C. 1985, ApJ, 292, 550
Pringle, J. E. 1981, ARA&A, 19, 137
Prinja, R. K., Long, K. S., Froning, C. S., Knigge, C., Witherick, D. K., Clark, J. S., & Ringwald, F. A. 2003, MNRAS, 340, 551
Rappaport, S., Verbunt, F., & Joss, P. C. 1983, ApJ, 275, 713
Retter, A., Leibowitz, E. M., & Naylor, T. 1999, MNRAS, 308, 140
Retter, A., & Naylor, T. 2000, MNRAS, 319, 510
Ritter, H., & Kolb, U. 2003, A&A, 404, 301
Rodríguez-Gil, P., Casares, J., Dhillon, V. S., & Martínez-Pais, I. G. 2000, A&A, 355, 181
Rodríguez-Gil, P., & Martínez-Pais, I. G. 2002, MNRAS, 337, 209
Rutten, R. G. M., van Paradijs, J., & Tinbergen, J. 1992, A&A, 260, 213
Selvelli, P., & Friedjung, M. 2003, A&A, 401, 297
Shakura, N. I., & Sunyaev, R. A. 1973, A&A, 24, 337
Shaviv, G., & Wehrse, R. 1986, A&A, 159, L5
Smith, D. A., Dhillon, V. S., & Marsh, T. R. 1998, MNRAS, 296, 465
Stickland, D. J., Kelly, B., Cooke, J. A., Coulson, I., Engelbrecht, C., Kilkenny, D., & Spencer-Jones, J. 1984, MNRAS, 206, 819
Szkody, P., Garnavich, P., Holberg, J., Silber, A., & Pastwick, L. 1997, AJ, 113, 2276
Taylor, C. J., Thorstensen, J. R., & Patterson, J. 1999, PASP, 111, 184
Taylor, C., et al. 1998, PASP, 110, 1148
Thoroughgood, T. D., Dhillon, V. S., Watson, C. A., Buckley, D. A., Steeghs, D., & Stevenson, M. J. 2004, MNRAS, 353, 1135
Tylenda, R. 1977, Acta Astron., 27, 235
———. 1981, Acta Astron., 31, 127
Vande, P., Smith, R., Hawkins, N. A., & Martin, J. S. 2003, MNRAS, 342, 151
Verbunt, F. 1997, MNRAS, 290, L55
Verbunt, F., Bunk, W. H., Ritter, H., & Pfeffermann, E. 1997, A&A, 327, 602
Verbunt, F., & Wade, R. A. 1984, A&AS, 57, 193
Wade, R. A. 1984, MNRAS, 208, 381
———. 1988, ApJ, 335, 394
Wade, R., & Hubeny, I. 1998, ApJ, 509, 350
Warner, B. 1986, MNRAS, 222, 11
———. 1987, MNRAS, 227, 23
Weight, A., Evans, A., Naylor, T., Wood, J. H., & Bode, M. F. 1994, MNRAS, 266, 761
Williams, G. A., & Shipman, H. L. 1988, ApJ, 326, 738
Williams, R. E. 1980, ApJ, 235, 939
Williams, R. E., & Ferguson, D. H. 1982, ApJ, 257, 672